Nanoscale

Accepted Manuscript

This article can be cited before page numbers have been issued, to do this please use: Y. Ji, M. Wang, Z. Yang, H. Qiu, S. Ji, J. Dou and N. V. Gaponenko, *Nanoscale*, 2020, DOI: 10.1039/D0NR00069H.

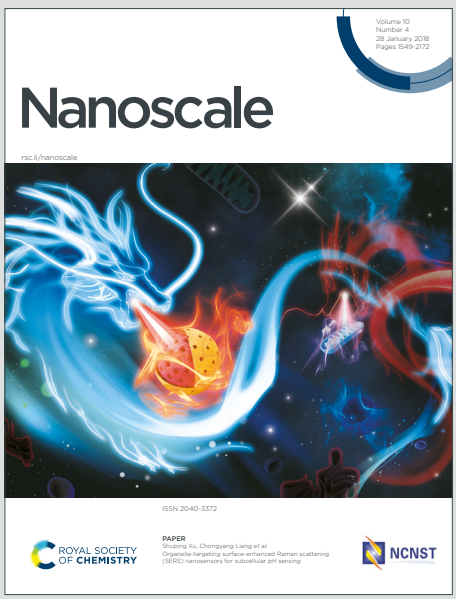

ROYAL SOCIETY OF CHEMISTRY

rsc.li/nanoscale

View Article Online
DOI: 10.1039/D0NR00069H

Nanoscale

PAPER

Highly Stable Na: $CsPb(Br, I)_3@Al_2O_3$ Nanocomposites Prepared by Pre-protection Strategy

.
0Received 00th January 20xx,
Accepted 00th January 20xx

DOI: 10.1039/x0xx00000x

Yongqiang Ji[a], Minqiang Wang*[a], Zhi Yang[a], Hengwei Qiu[a], Shangdong Ji[a], Jinjuan Dou[a], Nikolai V. Gaponenko[b]

Among the leading energy materials, metal tri-halide perovskite quantum dots (PQDs) with outstanding optoelectronic properties are still at the forefront of current research. However, the enormous challenges, including hazardous components and poor stability, remain to be addressed urgently problems before fulfilling its practical applications. Although there are diverse methods to improve the stability of PQDs, it is of central importance to avoid damage during operation. Herein, we develop a pre-protected strategy in which the coating combines the advantages of doping with sodium ions to jointly improve stability. Since the stable Na-rich surface acts as the defence, it protectes PQDs from damage during the coating process and therefore retains its initial fluorescence. When employing these Na-rich PQDs as core materials of coating, the highly fluorescent Na: $CsPb(Br,I)_3@Al_2O_3$ nanocomposites can maintain good stability even when directly immersed in water or exposed to illumination. Needless to say, the combination of these features sheds some light on the stabilization and applications of PQDs.

1. Introduction

Over a relatively short period of time, metal tri-halide PQDs ($CsPbX_3$; X = Cl, Br, or I) have an enormous level of interest throughout the scientific community due to their simple synthesis and excellent optical properties.[1-4] Further, their ultrahigh photoluminescence quantum yields (PLQYs), sharp emission and composition- and size-dependent band gap covering the entire visible spectrum,[5] especially solution processability and defect tolerance, make them attractive candidates not only for light-emitting diodes applications,[6-7] but also for other optoelectronic devices, such as solar cells,[8-9] photoconductor detectors, [10-11] and lasers.[12] Despite incredible advances in PQDs based photoelectric devices, the development of PQDs is still in its infancy stage. [13-14] Many challenges associated with such a system, for example, how to enhance unsatisfactory efficiency and how to improve poor stability of such PQDs, should be well settled before it can be applied in practical fields.[15-17]

Very recently, surface passivation by organic molecules has proven to be an efficient method to improve stability of PQDs.[18] However, the addition of such a dielectric coating will reduce the conductivity of PQDs films and therefore create an unfavorable electronic energy barrier for efficient charge injection or extraction in PQDs based optoelectronic devices.[19] In addition to surface passivation, it has been demonstrated that constructing heterostructures can also improve the stability of PQDs,[20-27] but large lattice mismatch between core and shell materials usually gives rise to the interfacial defects. Among the available materials, the most widely used coating material for colloidal QDs is silica because it possesses a wide tolerance window to core materials and provides needed robustness to overcome external perturbation.[20-23] However, tetraethyl orthosilicate

[a]*Electronic Materials Research Laboratory (EMRL), Key Laboratory of Education Ministry, International Center for Dielectric Research (ICDR),Shannxi Engineering Research Center of Advanced Energy Materials and Devices, School of Electronic and Information Engineering, Xi'an Jiaotong University, 710049 Xi'an, China. E-mail: mqwang@xjtu.edu.cn*
[b]*Belarusian State University of Informatics and Radioelectronics, P. Browki St.6, 220013 Minsk, Belarus*

(TEOS), as a precursor of silica for coating of traditional QDs such as carbon dots, CdSe and ZnS QDs, applied to PQDs failed in most attempts because the metal tri-halide PQDs belong to the class of soft matter system.[24] During water-assisted TEOS hydrolysis, the fluorescence of PQDs was quenched by water even before silica layers are formed on its surface.[25] Similarly, although TiO_2 produced by hydrolyzation of titanium butoxide significantly improved the stability of PQDs, it caused the PL to be degraded by nearly 90%.[26] In a nutshell, these methods are able to partly address the issue, such as the work reported by Zhang and co-workers.[17, 20] However, the probability of damaging PQDs during the coating process is greatly increased. Therefore, it is highly desired to develop a feasible method that can pre-protect PQDs from damage and retain its initial fluorescence during the post-processing process. It is worth mentioning that didodecyl dimethyl ammonium bromide (DDAB) can protect $CsPbBr_3$ (CPB) PQDs from damage during the coating process through enhanced bonds formed on the surface of PQDs.[27] However, DDAB is a sort of environmentally unfriendly reagent. Recent study also showed that potassium can also bond with halogen ions to form K-rich surface, thereby inhibiting the detachment of halogen ions from the surface of PQDs.[28] Later, PQDs added by Rb element demonstrated favorable properties, such as near-unity PLQYs and excellent stability, than that of bare PQDs.[29-31] Furthermore, the PL intensity of K-modified PQDs was almost the same as that of before the illumination even after 153 hours of continuous irradiation.[32] As a result, in addition to K and Rb elements, the introduction of the cost-efficient sodium element also significantly enhanced optical properties of PQDs.[33] However, to our best knowledge, there are no reports about the combination of PQDs coatings and doping to jointly improve stability.

Inspired by above-mentioned works, we develop a pre-protection strategy in this work, in which the coating combines the advantages of doping with sodium ions to jointly improve stability. As a consequence of this pre-protection strategy, these Na: $CsPb(Br, I)_3$@Al_2O_3 nanocomposites shows enhanced stability against moisture and illumination than that of the pristine PQDs.

Result and discussion

2.1 Stable Na-rich surface

The colloidal PQDs were synthesized according to a well-established synthesis process with minor modifications,[2] as illustrated in Fig. 1†. The concentrations of sodium were controlled by changing molar feeding ratios of Na_2CO_3 and Cs_2CO_3. All samples with different Na/Cs atom ratios were analysed by transmission electron microscopy (TEM). With the increasing ratio of Na/Cs (the feeding ratios of Na_2CO_3 to Cs_2CO_3 are 0, 0.11, 0.33, 1, and 3), it can be found that the PQDs can still retain a cubic morphology. The corresponding size distribution histograms further exhibit average diameters of 9.63, 11.04, 12.28, 12.58, and 13.36 nm, respectively, which is in good agreement with the TEM result, as displayed in Fig. S1†. The increase in particle size at high sodium content indicate that the increased ionicity of sodium over cesium could accelerate the speed of the reaction.[34] However, excess sodium leads to the formation of nanocages through a mechanism similar to the Kirkendall effect,[34] where pores are formed by decomposing the interior of PQDs under electron irradiation, showing that PQDs have more stable edges. As displayed in Fig. S2†, the lattice periodicity of individual nanocage can be seen, and the lattice spacing of ~0.29 nm is given, which is characteristic of the (200) plane of cubic CPB.[35] According to Stranks's work,[28] K-rich surface can be formed when potassium ions was added to the precursor of perovskite. Therefore, we believe that surface of nanocage is Na-rich, but still belongs to perovskite. Subsequently, STEM-elemental mapping was performed on sodium-containing sample, as shown in Fig. S3†. All of the corresponding mapping images of Cs, Pb, Br, and Na are overlapping with the STEM image, illustrating the existence of Na in the CPB PQDs, and the Cs/Pb/Br ratio of 1:1:3 is confirmed by energy-dispersive X-ray spectroscopy (EDS).

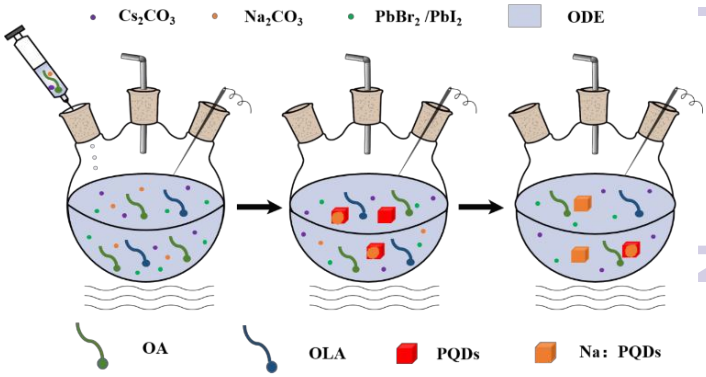

Fig. 1 Schematic diagram of the synthesis of Na: CPBI PQDs by hot injection method.

X-ray diffraction (XRD) patterns further confirmed that all peaks can be indexed as pure cubic phase (JCPDS card No.#54-0752), indicating a cubic crystal structure.[36] Furthermore, the peak intensity ratio of (110) at 21.55 and (100) at 15.18 increases with increasing ratio of Na/Cs,

which means that the addition of sodium contributes to the growth of PQDs along the (110) plane (Fig. S4a†). In the following section, the optical absorption and steady-state PL spectra of the colloidal Na: CPB PQDs with different Na/Cs atom ratios were measured and summarized, as shown in Fig. S4b†. One can see that the absorption edge shifts to the blue side without the introduction of any extra peaks as the proportion of ratio of Na/Cs increased, indicating that the introduction of sodium source does not change the spectra characteristics of PQDs but only shifted absorption peaks. As reported previously by several groups,[31, 33, 34] as the added alkali metal increases, the absorption peak shifts to high energy direction. Therefore, we believe that the contradiction between size increase and spectral blue shift may be due to the fact that the spectral effect associated with the sodium is stronger than that of the size. Like the trend of absorption spectra, the corresponding central emission peak changes from 529 to 497 nm. For a more detailed comparison, the PL intensity of the Na: CPB PQDs with different molar ratios were put together, as depicted in Fig. S4c†. It can be seen that their emission intensity increases at first and then decreases with an increase in Na/Cs ratio. When the Na/Cs ratio of 1/3 is employed, the maximum emission intensity is achieved with rather high PLQYs, but when Na/Cs ratio reaches 3, the PLQYs is seriously reduced, as plotted in Fig. S4d†.

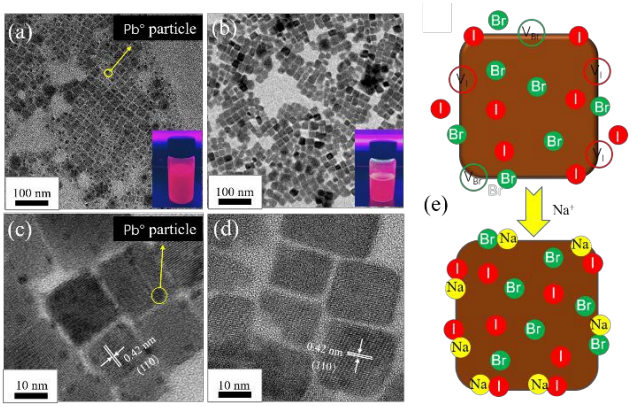

Fig. 2 (a, c) TEM and HRTEM images of CPBI PQDs. (b, d) TEM and HRTEM images of Na: CPBI PQDs. (e) Schematic representation of the formation of Na-rich surface of PQDs. (Na/Cs ratio is 0.33).

Many “black dots” with a much darker contrast are attached to the surface of the $CsPbBrI_2$ (CPBI) PQDs, as displayed in Fig. 2a, c. These “black dots” are often observed during TEM measurement when the electron beam is focused on the specimen for a long time. It is noteworthy that the increase of “black dots” often lead to the worse surface properties of PQDs, thereby reducing its optical performance.[37] Therefore, some researchers claimed that these “black dots” are decomposition product generated as electron-trapped surface sites through in situ reductions of PQDs,[37-40] and the as-observed “black dots” result in the rupture of periodic crystal lattice (Fig. S5†), that is, the chemical bonding between atoms are disconnected and remains as electron lone pair or vacant sites, producing a series of undesired nonradiative recombination pathways.[41] Therefore, in order to obtain a higher PLQYs, it is crucial to investigate the origin of "black dots", but so far there is still contradicting evidence regarding the nature of these "black dots".[37,39] Further investigations reveal that these "black dots" within PQDs surface can be completely converted into isolated "black dots" after 300 s of electron irradiation. Furthermore, the typical high resolution TEM (HRTEM) images of as-obtained isolated "black dots" demonstrated a lattice distance of 0.24 nm, which corresponds to the lattice distance of the (200) plane of metallic lead (Pb°),[40] as depicted in Fig. S6†. Subsequently, TEM images of the $PbBr_2$ solution before injection of cesium oleate, as expected, exhibits ultra-small particles, as shown in Fig. S7†, which is consistent with the report of Oran et al, they claimed that these ultra-small particles are Pb° particles, then verified in detail in their recent work.[39] Besides, in Li's latest work, they accurately demonstrated that these "black dots" are lead, not bromine or cesium enrichment, through STEM element mapping.[32] These results strongly support that these black dots" may belong to Pb° particles. In addition, we believe that these "black dots" can also be used as indicator of halogen vacancies, and suppression of "black dots" can reflect stable fluorescence on a single PQD. It is important to find that by adding sodium ions to the precursor of PQDs, the "black dots" attached to the surface of the PQDs can be suppressed, as shown in Fig. 2b, d. This is because these halide ions are immobilized through bonding with sodium ions to form a Na-rich surface, thereby inhibiting the detachment of halogen ions from the surface of PQDs, as illustrated in Fig. 2e, which is similar to the result of recent research.[28,42] Furthermore, the Na-rich PQDs have the same 0.42 nm lattice space as the pristine sample, which can be indexed to the (110) plane of the cubic phase (Fig. 2c, d).[43] In addition, the PL features of Na: CPBI PQDs, including the symmetric and sharp Gaussian shape, are consistent with the previous study, as shown in Fig. 3a.[44] Similarly, when Na/Cs ratio is 1/3, the PL intensity of Na: CPBI PQDs is significantly enhanced, with associated PLQYs of 82.21%, which is almost 1.6 times the pristine sample (Fig. S4e†), whereas no significant change is observed in the absorption spectra (Fig. S4f†).

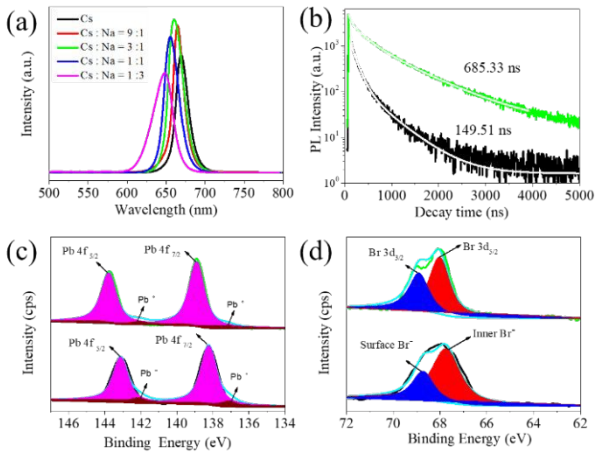

Fig. 3 (a) PL spectra (excitation at 365 nm) of Na: CPBI PQDs with different Na/Cs ratios. (b) Time-resolved PL decay curves. (c) HRXPS of Pb 4f. (d) HRXPS of Br 3d. (Na/Cs = 0.33). CPBI PQDs (black), Na: CPBI PQDs (green) and stmulated spectra (cyan).

To investigate how sodium ions affect the optical properties of PQDs, PL lifetimes of pristine and Na-rich samples are measured, as plotted in Fig. 3b, it is observed that the PL lifetime markedly enhances from 149.51 to 685.33 ns when the Na/Cs ratio of 1/3 is employed (Tab. 1), suggesting that a reduction in surface trap states occurred through introducing sodium. It is also an indication of good crystal quality with fewer defects for as-synthesized PQDs. In addition, X-ray photoelectron spectroscopy (XPS) was performed to elucidate the surface properties of PQDs with and without sodium. It was reported that the two contributions of the Pb 4f locating at 142.96 and 138.10 eV, corresponding to Pb^{2+}, respectively.[45] Further characterization reveals that by adding sodium ions to the precursor of PQDs, these additional components respect to Pb° at 137.2 and 142.1 eV are suppressed, as shown in Fig. 3c.[45] Subsequently, the Br 3d peaks were fitted into two peaks with binding energies of 68.2 and 69.1 eV for pristine PQDs and 68.4 and 69.3 eV for Na-rich PQDs, corresponding to the inner and surface bromine ions, respectively,[37] as plotted in Fig. 3d. Theoretically, for nanomaterials, larger particles have relatively fewer surface atoms than smaller particles. However, the intensity ratio of surface and inner bromine increases when the larger Na: CPBI PQDs are present, indicating that the surface of PQDs changed from a Pb°-rich state to a bromine-rich state, and in this process, non-radiative recombination on the surface are suppressed, which is evidenced by above-measured PLQYs and PL lifetimes. Furthermore, all element peaks shift to higher binding energy direction when the Na/Cs ratio of 1/3 is employed, indicating that the chemical bonds between the elements are enhanced (Fig. S8†).[8] Similarly, Cs_4PbBr_6 PQDs, also known as 0D QDs,[46-48] successfully suppress these "black dots" by the same way, as displayed in Fig. S9†, showing the general feasibility of this strategy. More importantly, the Na-rich PQDs have a slower halogen exchange compared to those of the pristine sample (Fig. S10†). It is worth pointing out that the addition of lithium is a better than sodium in improving stability. However, the optical properties of lithium-rich PQDs, including bandgap and lifetime, are difficult to adjust compared to other alkali metals. This may be because the equivalent cation formed by lithium and cesium hardly enters the crystal lattice of the perovskite, and therefore has a small effect on the properties of PQDs.

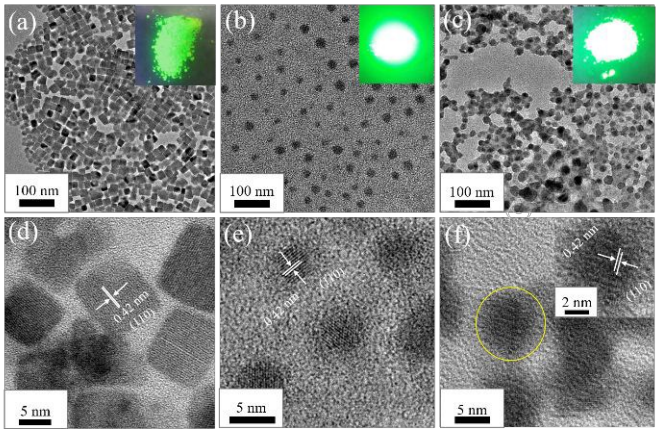

Fig. 4 TEM and HRTEM images of Na: CPB@Al_2O_3 product prepared at different ASB contents, respectively. (a, d) 10 µL, (b, e) 20 µL, and (c, f) 30 µL. (Inset) Digital images of the powder illuminated with 365 nm UV source. (Na/Cs ratio is 0.33).

2.2 Na: $CsPb(Br, I)_3@Al_2O_3$ microstructures

Since the stable Na-rich surface acts as the defense, it can prevent PQDs from decomposition during the post-processing process, so we tried to coat Na: CPB PQDs with aluminum sec-butoxide (ASB). As expected, ASB is successfully anchored to the surface of Na: CPB PQDs, as evidenced by subsequent morphological change. If the amount of 20 µL ASB is provided, alloy structure is exactly formed and each PQD is exactly incorporated in alumina (Fig. 4b, e). When the amount of ASB is decreased to half of 20 µL, the edges of the PQD become blurred, which may be related to the thin alumina layers formed on the surface of PQDs, as shown in Fig. 4a, d. Further raising ASB to 30 µL lead to the formation of the big aggregates, multiple Na: CPB PQDs will be simultaneously encapsulated in a big amorphous alumina, as displayed in Fig. 4c, f. Importantly, 1024 mg of highly stable Na: CPB@Al_2O_3 PQDs powder

was successfully obtained in one batch (Fig. S11†), indicating better fluorescence emission than other samples under a 365 nm UV source (inset Fig. 4). Based on above-mentioned observations, we propose a plausible coating mechanism, as illustrated in Fig. S12†. When ASB is deposited on the surface of PQDs, PQDs-ASB complexes with full contact will be completed, followed by hydrolysis to generate thin alumina layers on the surface of PQDs. Accompanied by the formation of alumina shell, the shape of the PQDs changes from cube to the sphere, which may be due to a trace amount of water on the PQDs surface produced, and reacted with the corners and edges as they are the most active sites, as evidenced by a series of HRTEM images of PQDs with continuously changing morphology (Fig. S13†). It is worth noting that fluorescence of PQDs was not quenched during the coating process, proving the feasibility of our pre-protection strategy (Fig. S14a†). In addition, the XRD pattern of the coating sample appears several additional broad peaks with respect to the standard diffraction pattern of cubic CPB phase, which may correspond to alumina, is not present in the diffraction pattern of the as-prepared pristine sample, as shown in Fig S14b †. The other diffraction peaks can be indexed as pure cubic phase (JCPDS card No.#54-0752), suggesting that the crystal structure remained unchanged during the coating process, which is consistent with invariant lattice spacing from HRTEM image, as plotted in Fig. 4e†. Subsequently, the Fourier transform infrared spectroscopy was applied to analyze purified samples with and without alumina coating, of which the result is displayed in Fig. S14c†. Some additional peaks centred around 594 cm^{-1} and 3450 cm^{-1} appeared in the coated samples, which may correspond to the alumina produced by the hydrolysis of ASB,[49] confirmed that the surface of the PQD was successfully coated with alumina, which was further confirmed by elemental analysis of the EDS patterns of the purified sample, as plotted in Fig. S14d†.

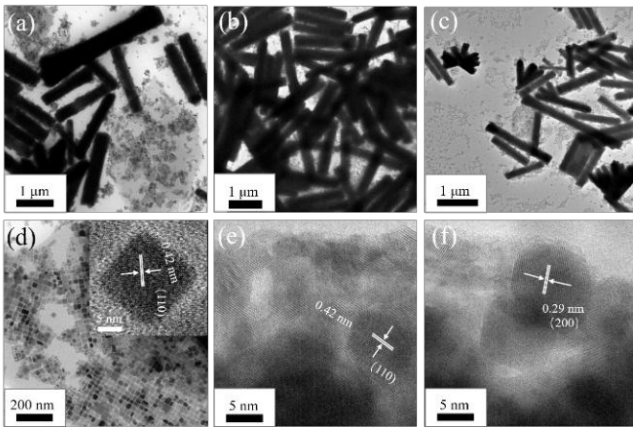

Fig. 5 TEM and HRTEM images of Na: CPBI@Al_2O_3 product prepared at different ASB contents, respectively. (a, d) 10 μL, (b, e) 20 μL, and (c, f) 30 μL. (Na/Cs ratio is 0.33).

The same strategy is extended to CPBI PQDs, which is different from the CPB PQDs that shows declined emission, accompanied by a noticeable colour change, as shown in Fig. S15†, suggesting that the CPBI PQDs may already be converted into another structure, which may be due to the highly labile ionic structure of CPBI PQDs. Subsequently, TEM analysis reveals that when 10 μL ASB is provided, most of the products are nanorods (NRs), along with PQDs embedded in alumina (Fig. 5a). More attractively, the embedded PQDs retain its initial lattice spacing of 0.42 nm, as displayed in Fig. 5d. Further investigation reveals that when the amount of ASB is increased to 20 μL, the CPBI PQDs are completely converted into NRs (Fig. 5b). As indicated by TEM, the thickness of isolated nanorods is estimated to be 300 nm and a length of up to several micrometers. Specifically, these embedded PQDs that may had been already produced at an early stage were subsequently assembled into NRs. To put it simply, extra ASB triggers these embedded PQDs, allows them to further shorten their distance until they touch each other and then fuse to NRs through lattice matching, as evidenced by the HRTEM image (Fig. S16†). Although the corners and edges of cube disappear, these fused PQDs have the same lattice spacing as the pristine sample (Fig. 5e). If the amount of ASB is further increased to 30 μL, the lattice spacing of NRs changes from 0.42 to 0.29 nm (Fig. 5f), with associated morphological change, as shown in Fig. 5c. As a result, some superstructures analogous to the paper mulberry as well as its intermediates were produced, as shown in Fig. S17-18†. Based on above-mentioned observations, it is reasonable to believe that these superstructures are constructed by self-assembly of NRs, and these NRs are aligned perpendicularly to the spherical surface, pointing to a common centre. Furthermore, these target elements have a clear elemental paper mulberry microscopic profile (Fig. 6), and the Cs/Pb/Br/I/ ratio is slightly 1:1:1:2 (Fig. S19†), indicating that the stoichiometry is well preserved in superstructures. According to our previous work,[50] polar molecules, such as ASB, cna cause lattice distortion and thus produce dipole-dipole interactions, which make CPBI PQDs firstly self-assemble into NRs, then intermediates, and finally to paper mulberrye superstructures. In addition, all types of CPBI PQDs exhibit XPS peaks of Cs, Pb, Br and I. However, additional peaks in CPBI PQDs synthesized with sodium appeared at 1071.4 eV, which could be

View Article Online
DOI: 10.1039/D0NR00068H

assigned to the Na 1s signals of Na^+, proving that Na^+ existed into CPBI PQD (Fig. S20a†). This is further supported by the high-resolution XPS spectra of Na 1s shown in Fig. S20d†. Furthermore, the Al 2p peak at 74.7 eV and the O 1s peak at 531.6 eV can be indexed as the binding energies of alumina (Fig. S20b, c†). Subsequently, the high-resolution XPS spectrum of O 1s is deconvoluted into two different peaks, with the main peak is attributed to the O of alumina and the minor peak is assigned to the hydroxyl group, where binding energies at ≈530.7 and 533.9 eV, respectively, as shown in Fig. S21a†.[26] However, the hydroxyl peak completely disappear after annealing at 50 °C for 60 min (Fig. S20b†). It is worth pointing out that when ASB was added to CPBI PQDs solution, the colour of the solution immediately changed from red to colourless. Subsequently, element distribution of microstructure of the solution was revealed by SEM-elemental mapping. With the exception of O and Al, perovskite element all demonstrate clear elemental profiles, as shown in Fig. S22†.

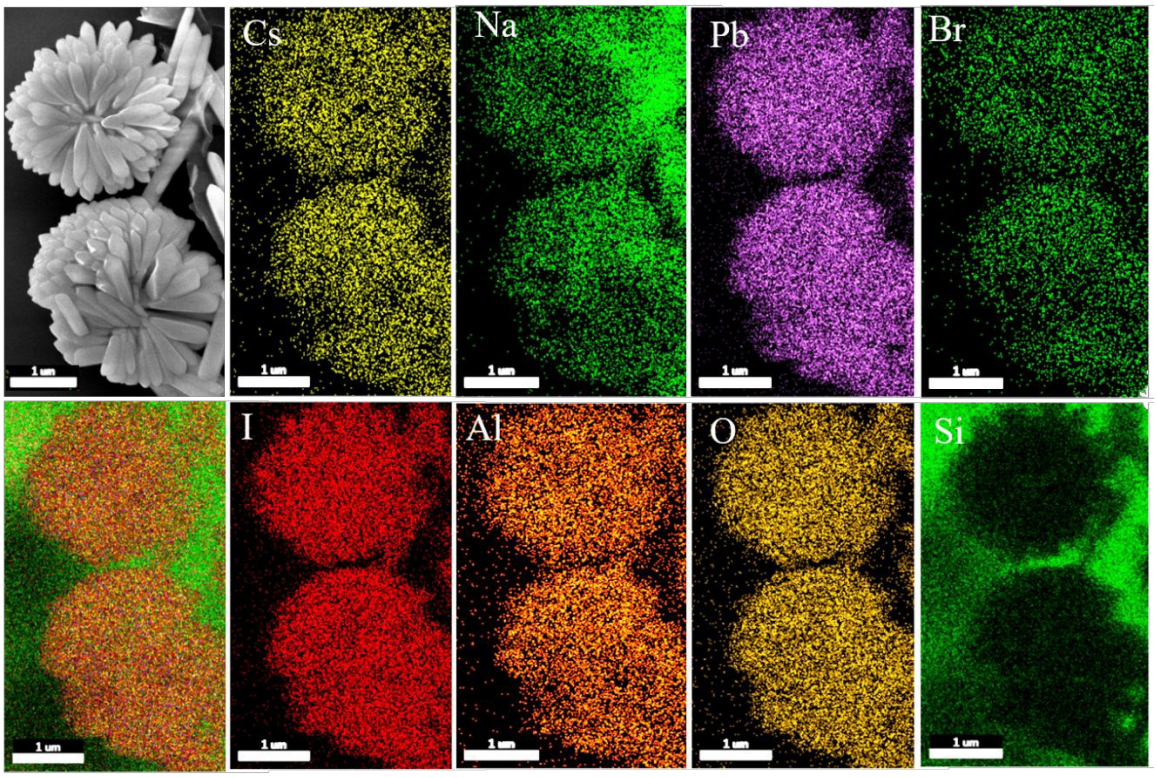

Fig. 6 SEM image of paper mulberry-like superstructure profile and their corresponding elemental mapping images showing the element distributions of Cs, Na, Pb, Br, I, Al, O, Si and overlapping elements.

2.3 Stability

The stability of PQDs was constantly monitored by measuring its PL intensity, which has been frequently used in previous work.[51-55] As shown in Fig 7a, it can be found that PL intensity of CPB PQDs drops rapidly in water under ultrasonication, and the corresponding green emission becomes weak after 20 min and then almost disappear after 40 min (Fig. S23†). In a striking contrast, the PL intensity of Na: CPB@Al_2O_3 PQDs shows a higher stability to water (Fig 7b). Despite their poor dispersion in water, bright emission could still be observed under UV source after the same treatment for 40 min (Fig. S23†), confirming the improved stability. Similar enhancement effects have been reported in core/shell of PQDs, such as CPB/ZrO_2 and CPB/SiO_2 PQDs.[17,51] It was already established that the light can convert oxygen into anion O^{2-} via light-assisted ionization.[24] These O^{2-} species can easily occupy halide vacancy sites, resulting in high surface defect density of PQDs without emission.[53] However, the Na: CPB@Al_2O_3 PQDs is nearly the same as that of before the illumination even after 72 h of continuous irradiation under UV source (Fig.S24a†). This is because coated PQDs are isolated from external perturbations by alumina.[54] Although the

View Article Online
DOI: 10.1039/D0NR00069H

fluorescence was quenched after the addition of water, the fluorescence quenching of the Na: CPBI @Al_2O_3 nanocomposites is much slower than that of pristine sample (Fig. S24b†). More attractively, the emission from the CPBI PQDs sharply drops at the start of illumination and then decreases to approximately 20% of the initial intensity after 5 h of continuous illumination (Fig 7d). By contrast, the emission intensity of Na: CPBI@Al_2O_3 nanocomposites can maintain approximately 80% of the initial intensity after the same treatment even 16 h (Fig. 7e). Along with the change in PL intensity, the emission change of the both samples under UV source is shown in Fig. S25†.

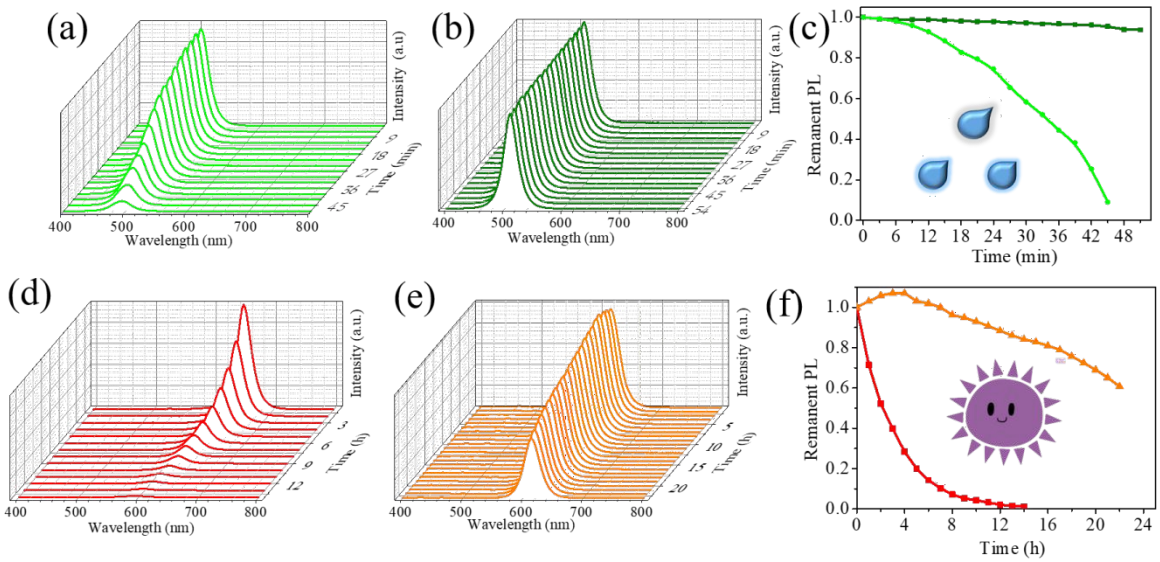

Fig. 7 Change in PL intensity under different treatment. Ten milligram samples were dispersed in 2 mL of deionized water under ultrasonication.(a) CPB PQDs. (b) Na: CPB@Al_2O_3 PQDs. Two samples were stimulated through illuminating the solution with a portable UV lamp (365 nm, 10 W) at 3 cm distance. (d) CPBI PQDs. (e) Na: CPBI@Al_2O_3 nanocomposites. (c, f) the comparison of relative PL intensity for different samples.

Conclusions

In summary, we develop a pre-protected strategy in which the coating combines the advantages of doping with sodium ions to jointly improve stability. Since the stable Na-rich surface act as the defence, the contradiction of coating PQDs between high stability and fluorescence quenching is well addressed. Consequently, Na: $CsPb(Br, I)_3$@Al_2O_3 nanocomposites demonstrated substantially improved environmental stability. As a result of this understanding, our work not only provides a universal approach for PQDs pre-protection that can be extended to other materials with various components but also sheds some light on the stabilization and applications of PQDs.

Conflicts of interest

There are no conflicts to declare

Acknowledgements

We thank Ms. Yanzhu Dai at International Center for Dielectric Research (ICDR) for her help in using FESEM and Jiamei Liu at Instrument Analysis Center of Xi'an Jiaotong University for her help with XPS analysis, respectively. This work was supported by the National Natural Science Foundation of China (NSFC, 61774124, 51572216 and 61604122), the Fundamental Research Funds for the Central Universities (1191329876 and 1191329152), the 111 Plan (B14040), the China postdoctoral Science Foundation (2019M660253), and the Innovation Capability Support Program of Shannxi (No.2018PT-28, 2019PT-05).

References

1 Q. A. Akkerman, V. D'Innocenzo, S. Accornero, A. Scarpellini, A. Petrozza, M, Prato and L. Manna, J. Am. Chem. Soc., 2015, 137, 10276-10281.

2 L. Protesescu, S. Yakunin, M. I. Bodnarchuk, F. Krieg, R. Caputo, C. H. Hendon, R. X. Yang, A. Walsh and M. V. Kovalenko, Nano Lett., 2015, 15, 3692-3696.
3 J. Shamsi, A. S. Urban, M. Imran, L. D. Trizio and L. Manna, Chem. Rev., 2019, 119, 3296-3348.
4 L. Polavarapu, Q Zhang and R. Krahne, Nanoscale., 2019, 11, 8648-8650.
5 D. Yang, M. Cao, Q. Zhong, P. Li, X. Zhang and Q. Zhang, J. Mater. Chem. C., 2019, 7, 757-789.
6 H. Wu, Y. Zhang, M. Lu, X. Zhang, C. Sun, T. Zhang, V. L. Colvin and W. W. Yu, Nanoscale., 2018, 10, 4173-4178.
7 F. Palazon, F. D. Stasio, Q. A. Akkerman, R. Krahne, M. Prato and L. Manna, Chem. Mater., 2016, 28, 2902-2906.
8 J. Yuan, X. Ling, D. Yang, F. Li, S. Zhou, J. Shi, Y. Qian, J. Hu, Y. Sun, Y. Yang, X. Gao, S. Duhm, Q. Zhang and W. Ma, Joule., 2018, 2, 2450-2463.
9 Q. A. Akkerman, M. Gandini, F. Di Stasio, P. Rastogi, F. Palazon, G. Bertoni, J. M. Ball, M. Prato, A. Petrozza and L. Manna, Nat. Energy., 2016, 2, 16194.
10 W. Zhai, J. Lin, C. Li, S. Hu, Y. Huang, C. Yu, Z. Wen, Z. Liu, Y. Fang and C. Tan, Nanoscale., 2018, 10, 21451-21458.
11 Z. Yang, J. Dou, M. Wang, J. Li, J. Huang and J. Shao, J. Mater. Chem. C., 2018, 6, 6739-6746.
12 L. Zhang, F. Yuan, H. Dong, B. Jiao, W. Zhang, X. Hou, S. Wang, Q. Gong and Z. Wu, ACS Appl. Mater. Interfaces., 2018, 10, 40661-40671.
13 Y. Wei, X. Deng, Z. Xie, X. Cai, S. Liang, P. Ma, Z. Hou, Z. Cheng and J. Lin, Adv. Funct. Mater., 2017, 27, 1703535.
14 Q. A. Akkerman, G. Rainò, M. V. Kovalenko and L. Manna, Nat. Mater., 2018, 17, 394-405.
15 Q. Zhang and Y. Yin, ACS Central Sci., 2018, 4, 668-679.
16 Y. Wei, Z. Cheng and J. Lin, Chem. Soc. Rev., 2019, 48, 310-350
17 H. Liu, Y. Tan, M. Cao, H. Hu, L. Wu, X. Yu, L. Wang, B. Sun and Q. Zhang, ACS Nano., 2019, 13, 5366-5374.
18 C. Zhang, B Wang, Q. Wan, L Kong, W Zheng, Z. Lia and L. Li, Nanoscale., 2019, 11, 2602-2607.
19 X. Shen, C. Sun, X. Bai, X. Zhang, Y. Wang, Y. Wang, H. Song and W. W. Yu, ACS Appl. Mater. Interfaces., 2018, 10, 16768-16775.
20 H. Hu, L. Wu, Y. Tan, Q. Zhong, M. Chen, Y. Qiu, D. Yang, B. Sun, Q. Zhang and Y. Yin, J. Am. Chem. Soc., 2018, 140, 406-412.
21 W. Chen, J. Hao, W. Hu, Z. Zang, X. Tang, L. Fang, T. Niu and M. Zhou, Small., 2017, 13, 1604085.
22 S. Huang, Z. Li, L. Kong, N. Zhu, A. Shan and L. Li, J. Am. Chem. Soc., 2016, 138, 5749-5752.
23 X. Tang, W. Chen, Z. Liu, J. Du, Z. Yao, Y. Huang, C. Chen, Z. Yang, T. Shi, W. Hu, Z. Zang, Y. Chen and Y. Leng, Small., 2019, 15, 1900484.
24 W. Lv, L. Li, M. Xu, J. Hong, X. Tang, L. Xu, Y. Wu, R. Zhu, R. Chen and W. Huang, Adv. Mater., 2019, 31, 1900682.
25 J. Cai, K. Gu, Y. Zhu, J. Zhu, Y. Wang, J. Shen, A. Trinchi, C. Li and G. Wei, Chem. Commun., 2018, 54, 8064-8067.
26 Z. Li, E. Hofman, J. Li, A. Davis, C. Tung, L. Wu and W. Zheng, Adv. Funct. Mater., 2017, 28, 1704288.
27 Z. Li, L. Kong, S. Huang and L. Li, Angew. Chem. Int. Ed., 2017, 129, 8246 -8250.
28 M. Abdi-Jalebi, Z. Andaji-Garmaroudi, S. Cacovich, C. Stavrakas, B. Philippe, J. M. Richter, M. Alsari, E. P. Booker, E. M. Hutter, A. J. Pearson, S. Lilliu, T. J. Savenije, H. Rensmo, G. Divitini, C. Ducati, R. H. Friend and S. D. Stranks, Nature., 2018, 555, 497-501.
29 T. J. Jacobsson, S. Svanstr om, V. Andrei, J. P. H. Rivett, N. Kornienko, B. Philippe, U. B. Cappel, H. Rensmo, F. Deschler and G. Boschloo, J. Phys. Chem. C., 2018, 122, 13548-13557.
30 F. Meng, X. Liu, X. Cai, Z. Gong, B. Li, W. Xie, M. Li, D. Chen, H. Yip and S. Su, Nanoscale., 2019, 11, 1295-1303.
31 H. Wu, Y. Yang, D. Zhou, K. Li, J. Yu, J. Han, Z. Li, Z. Long, J. Ma and J. Qiu, Nanoscale., 2018, 10, 3429-3437.
32 S. Huang, B. Wang, Q. Zhang, Z. Li, A. Shan and L. Li, Adv. Opt. Mater., 2018, 6, 1701106.
33 S. Li, Z. Shi, F. Zhang, L. Wang, Z. Ma, D. Yang, Z. Yao, D. Wu, T. Xu, Y. Tian, Y. Zhang, C. Shan and X. J. Li, Chem. Mater., 2019, 31, 3917-3928.
34 Y. Liu, G. Pan, R. Wang, H. Shao, H. Wang, W. Xu, H. Cui and H. Son. Nanoscale., 2018, 10, 14067-14072.
35 Y. Wei, K. Li, Z. Cheng, M. Liu, H. Xiao, P. Dang, S. Liang, Z. Wu, H. Lian and J. Lin, Adv. Mater., 2019, 13, 1807592.
36 Y. ji, M. Wang, Z. Yang, S. Ji and H. Qiu, J. Mater. Chem. C., 2019, 7, 8471-8476.
37 F. Li, Y. Liu, H. Wang, Q. Zhan, Q. Liu and Z. Xia, Chem. Mater., 2018, 30, 8546-8554.
38 A. Kostopoulou, M. Sygletou, K. Brintakis, A. Lappas and E. Stratakis, Nanoscale., 2017, 9, 18202-18207.
39 T. Udayabhaskararao, M. Kazes, L. Houben, H. Lin and D. Oron, Chem. Mater., 2017, 29, 1302-1308.
40 M. Zhang, H. Li, Q. Jing, Z. Lu and P. Wang, Crystals., 2018, 8, 2.
41 J. Lim, W K Bae, J. Kwak, S Lee, C Lee and K. Char, Opt Mater Express., 2012, 2, 594-628.
42 B. Wang, C. Zhang, S. Huang, Z. Li, L Kong, L. Jin, J. Wang, K. Wu and L. Li, ACS Appl. Mater. Interfaces., 2018, 10, 23303-23310.
43 L. Wu, H. Hu, Y. Xu, S. Jiang, M. Chen, Q. Zhong, D. Yang, Q. Liu, Y. Zhao, B. Sun, Q. Zhang and Y. Yin, Nano Lett., 2017, 17, 5799-5804
44 J. Zhang, L. Zhang, P Cai, X. Xue, M. Wang, J Zhang and G. Tu, Nano Energy., 2019, 62, 434-44.
45 S. Yuan, Z. Wang, M. Zhuo, Q. Tian, Y. Jin and L. Liao, ACS Nano., 2018, 12, 9541-9548.
46 Q. A. Akkerman, Ahmed. L. Abdelhady and L. Mann, J. Phys. Chem. Lett., 2018, 9, 2326-2337.
47 Z. Liu, Y. Bekenstein, X. Ye, S. C. Nguyen, J. Swabeck, D. Zhang, S. Lee, P. Yang, W. Ma and A. P. Alivisatos, J. Am. Chem. Soc., 2017, 139, 5309-5312.
48 Q. A. Akkerman, S. Park, E. Radicchi, F. Nunzi, E. Mosconi, F. D. Angelis, R. Brescia, P. Rastogi, M Prato and L. Manna, Nano Lett., 2017, 17, 1924-1930.
49 A. Loiudice, S. Saris, E. Oveisi, D. T. L. Alexander and R. Buonsanti, Angew. Chem. Int. Ed., 2017, 56, 10696-10701.
50 Y. Ji, M. Wang, Z. Yang, S. Ji, H. Qiu, J. Doua and N.V. Gaponenko, Chem. Commun., 2019, 55, 12809-12812.

51 Q. Zhong, M. Cao, H. Hu, D. Yang, M. Chen, P. Li, L. Wu and Q. Zhang, ACS Nano., 2018, 12, 8579-8587.

52 P. Chen, Y. Liu, Z. Zhang, Y. Sun, J. Hou, G. Zhao, J. Zou, Y. Fang, J. Xu and N. Dai, Nanoscale., 2019, 11, 16499-1650

53 J. Zhang, X. Liu, P. Jiang, H. Chen, Y. Wang, J. Ma, R. Zhang, F. Yang, M. Wang, J. Zhang and G. Tu, Nano Energy., 2019, 66, 104142.

54 S. Park, M. N. An, G. Almeida, F. Palazon, D. Spirito, R. Krahne, Z. Dang, L. D. Trizio and L. Manna, Nanoscale., 2019, 11, 18739-18745.

55 Q. Zhong, M. Cao, Y. Xu, P. Li, Y. Zhang, H. Hu, D. Yang, Y. Xu, L. Wang, Y. Li, X. Zhang and Q. Zhang, Nano Lett., 2019, 19, 4151-4157.